



Gotte, J.B., O'Holleran, K. , Preece, D., Flossmann, F., Franke-Arnold, S. , Barnett, S.M., and Padgett, M.J. (2008) *Light beams with fractional orbital angular momentum and their vortex structure*. Optics Express, 16 (2). pp. 993-1006. ISSN 1094-4087 (doi:10.1364/OE.16.000993)

<http://eprints.gla.ac.uk/32367/>

Deposited on: 11th September 2012

Light beams with fractional orbital angular momentum and their vortex structure

Jörg B. Götte¹, Kevin O'Holleran¹, Daryl Preece¹, Florian Flossmann¹,
Sonja Franke-Arnold¹, Stephen M. Barnett² and Miles J. Padgett¹

¹ Department of Physics and Astronomy, SUPA, University of Glasgow, Glasgow G12 8QQ, UK

² Department of Physics, SUPA, University of Strathclyde, Glasgow G4 0NG, UK.

m.padgett@physics.gla.ac.uk

Abstract: Light emerging from a spiral phase plate with a non-integer phase step has a complicated vortex structure and is unstable on propagation. We generate light carrying fractional orbital angular momentum (OAM) not with a phase step but by a synthesis of Laguerre-Gaussian modes. By limiting the number of different Gouy phases in the superposition we produce a light beam which is well characterised in terms of its propagation. We believe that their structural stability makes these beams ideal for quantum information processes utilising fractional OAM states.

© 2008 Optical Society of America

OCIS codes: (350.5030) Phase; (050.4865) Optical vortices; (260.6042) Singular optics; (090.1760) Computer Holography; (230.6120) Spatial light modulators; (270.0270) Quantum optics.

References and links

1. M. V. Berry, "Much ado about nothing: optical distortion lines (phase singularities, zeros, and vortices)," in *International Conference on Singular Optics*, M. S. Soskin, ed., Proc. SPIE **3487**, 1–5 (1998). http://spie.org/x648.xml?product_id=317693.
2. M. V. Berry and M. R. Dennis, "Knotted and linked phase singularities in monochromatic waves," Proc. Royal Society of London, Series A **457**(2013), 2251–2263 (2001). <http://www.journals.royalsoc.ac.uk/content/yv6lqeufbq2phg91>.
3. J. Leach, M. R. Dennis, and M. J. Padgett, "Laser beams: Knotted threads of darkness," Nature **432**(165) (2004). <http://www.nature.com/nature/journal/v432/n7014/abs/432165a.html>.
4. J. Leach, M. R. Dennis, J. Courtial, and M. Padgett, "Vortex knots in light," New J. Phys. **7**, 55 (2005). <http://www.iop.org/EJ/abstract/1367-2630/7/1/055/>.
5. L. Allen, M. W. Beijersbergen, R. J. C. Spreeuw, and J. P. Woerdman, "Orbital angular momentum of light and the transformation of Laguerre-Gaussian modes," Phys. Rev. A **45**, 8185–8190 (1992). <http://link.aps.org/abstract/PRA/v45/p8185>.
6. L. Allen and M. J. Padgett, "The Poynting vector in Laguerre-Gaussian beams and the interpretation of their angular momentum density," Opt. Commun. **184**, 67–71 (2000).
7. M. W. Beijersbergen, R. P. C. Coerwinkel, M. Kristensen, and J. P. Woerdman, "Helical-wavefront next term laser beams produced with a spiral phaseplate," Opt. Commun. **112**, 321–327 (1994).
8. V. Y. Bazhenov, M. V. Vastnetsov, and M. S. Soskin, "Laser-beams with screw dislocations in their wave-fronts," JETP Lett. **52**, 429–431 (1990).
9. M. V. Berry, "Optical vortices evolving from helicoidal integer and fractional phase steps," J. Opt. A **6**, 259–269 (2004). <http://www.iop.org/EJ/abstract/1464-4258/6/2/018>.
10. J. Leach, E. Yao, and M. J. Padgett, "Observation of the vortex structure of a non-integer vortex beam," New J. Phys. **6**, 71 (2004). <http://www.iop.org/EJ/abstract/1367-2630/6/1/071/>.
11. K. O'Holleran, M. R. Dennis, and M. J. Padgett, "Illustrations of optical vortices in three dimensions," Journal of European Optical Society - Rapid Publications **1**, 06008 (2006). https://www.jeos.org/index.php/jeos_rp/article/view/06008.

12. J. Götze, S. Franke-Arnold, R. Zambrini, and S. M. Barnett, "Quantum formulation of fractional orbital angular momentum," *J. Mod. Opt.* **54**, 1723–1738 (2007). <http://www.informaworld.com/smpp/content~content=a779773614>.
13. S. S. R. Oemrawsingh, A. Aiello, E. R. Eliel, G. Nienhaus, and J. P. Woerdman, "How to observe High-Dimensional Two-Photon Entanglement with Only Two Detectors," *Physical Review Letters* **92**, 217901 (2004). <http://link.aps.org/abstract/PRL/v92/e217901>.
14. G. F. Calvo, A. Picón, and A. Bramon, "Measuring two-photon orbital angular momentum entanglement," *Phys. Rev. A* **75**, 012319 (2007). <http://link.aps.org/abstract/PRA/v75/e012319>.
15. A. Aiello, S. S. R. Oemrawsingh, E. R. Eliel, and J. P. Woerdman, "Nonlocality of high-dimensional two-photon orbital angular momentum states," *Phys. Rev. A* **72**, 052114 (2005). <http://link.aps.org/abstract/PRA/v72/e052114>.
16. S. M. Barnett and D. T. Pegg, "Quantum theory of rotation angles," *Phys. Rev. A* **41**, 3427–3435 (1990). <http://link.aps.org/abstract/PRA/v41/p3427>.
17. J. Courtial, "Self-imaging beams and the Guoy [*sic*] effect," *Opt. Commun.* **151**, 1–4 (1998).
18. R. Zambrini, L. C. Thomson, S. M. Barnett, and M. Padgett, "Momentum paradox in a vortex core," *J. Modern Opt.* **52**(8), 1135–1144 (2005). <http://www.informaworld.com/smpp/content~content=a713736931>.
19. C. Alonzo, P. J. Rodrigo and J. Glückstad, "Helico-conical optical beams: a product of helical and conical phase fronts," *Opt. Express.* **13**, 1749–1760 (2005). <http://www.opticsexpress.org/abstract.cfm?URI=oe-13-5-1749>.

1. Introduction

Optical vortices are phase singularities which are formed when light waves or beams are superposed [1]. In three dimensions these points of complete destructive interference trace out connected structures such as loops and knots [2, 3, 4]. The study of optical vortices is closely related to the field of orbital angular momentum (OAM) of light. Light beams with an azimuthal phase structure $\exp(im\phi)$, where m is an integer number, carry OAM of $m\hbar$ per photon [5], which arises directly from the azimuthal component of their Poynting vector [6]. A common example for such light beams are the Laguerre-Gaussian (LG) modes, which can be produced in the laboratory using spiral phase plates [7] or computer generated holograms [8]. Optical components which generate LG beams imprint a $2\pi m$ step in the phase of the electromagnetic field. However, it is also possible to design the step so that the phase jump is not an integer multiple of 2π . This gives rise to the phenomenon of non-integer, or fractional, OAM. Within the scope of our study irrational numbers are of no particular importance and we often use 'fractional', where 'non-integer' would be more complete. The vortex structure of light emerging from a non-integer phase step was first studied by Berry [9]. It is characterised by a chain of alternating vortices which forms in a dark line associated with the edge dislocation of the phase [10]. If one looks at the vortex structure in three dimensions one can see that every pair of alternating vortices in this chain is part of a nodal line in form of a 'hairpin', that is the two vortices converge at a common 'turning point' [11]. This chain of vortices affects the intensity and phase profiles of light emerging from a fractional phase step and makes the light unstable on propagation.

A different way to produce light with fractional OAM is as a generic superposition of light modes with different values of m . Using the correspondence between optics and quantum theory we have found a representation of light with fractional OAM as a quantum state. This state can be decomposed into a basis of integer OAM states [12]. The decomposition only determines the OAM index m , which in a superposition of LG beams leaves the index for the number of concentric rings unspecified. In this paper we make use of this flexibility to find a representation of a fractional OAM state in terms of LG beams with a minimal number of different Gouy phases to increase propagational stability. We produce these beams using a spatial light modulator (SLM) and study their propagation and vortex structure. Light beams constructed in this way are an excellent realisation of non-integer OAM states and they are more stable on propagation than light emerging from fractional phase steps.

Spiral phase plates and light beams carrying non-integer OAM have also been studied in the context of two photon entanglement [13, 14]. Experiments in this area could benefit greatly from an enhanced propagation distance for the light beams with fractional OAM.

2. Construction of light beams with non-integer OAM

We denote the state representing light emerging from a fractional phase step with $|M(\alpha)\rangle$, where $M = m + \mu$ and m is the integer part and μ lies between 0 and 1. Unlike integer OAM states, which are fully characterised by the OAM index m , these fractional OAM states also depend on the orientation of the edge dislocation α [13, 15]. These states can be decomposed into the basis of integer OAM states according to

$$|M(\alpha)\rangle = \sum_{m'} c_{m'} [M(\alpha)] |m\rangle, \quad (1)$$

where the coefficients $c_{m'} [M(\alpha)]$ are given by [12]

$$c_{m'} [M(\alpha)] = \exp(-i\mu\alpha) \frac{i \exp[i(M - m')\theta_0]}{2\pi(M - m')} [\exp[i(M - m')\alpha] (1 - \exp(i\mu 2\pi))]. \quad (2)$$

The angle θ_0 is an arbitrary starting point which defines the interval $\theta_0 \leq \phi < \theta_0 + 2\pi$ for the azimuthal angle ϕ [16]. The orientation of the edge dislocation α is measured from θ_0 , so that α lies always between 0 and 2π . Although arbitrary, θ_0 defines one basis set for the angle and it is important to keep in mind that non-integer OAM states in general are different for different choices of θ_0 . In the remainder of this paper we set θ_0 to $-\pi$. We should stress that in the construction of the fractional OAM state (1) we have taken great care to avoid a multi-valued behaviour as known from complex analysis and easily associated with a fractional phase [12]. In the following we construct a physical representation of Eq. (1). The LHS is represented by the light field $\Psi_{M(\alpha)}$ emerging from a fractional phase step with the phase discontinuity oriented at α . The RHS is a weighted superposition of integer OAM states. As we want to use the Gouy phase to control the vortex structure we use the complete set of LG modes u_p^m as implementation of integer OAM states. In cylindrical coordinates the field amplitude of the LG mode is given by:

$$u_p^m(\rho, \phi, z) \propto \frac{C_{mp}}{\sqrt{w(z)}} \left(\frac{\rho\sqrt{2}}{w(z)} \right)^{|m|} \exp\left(-\frac{\rho^2}{w^2(z)}\right) L_p^{|m|} \left(\frac{2\rho^2}{w^2(z)} \right) \times \exp\left(i\frac{\rho^2}{w^2(z)} \frac{z}{z_R}\right) \exp(im\phi) \exp[-i(2p + |m| + 1) \tan^{-1}(z/z_R)], \quad (3)$$

where $w(z)$ is the Gaussian spot size

$$w(z) = \sqrt{2 \frac{z_R^2 + z^2}{kz_R}} = w_0 \sqrt{1 + \frac{z^2}{z_R^2}}, \quad (4)$$

k denotes the wavenumber, z_R the Rayleigh range, w_0 the beam waist and $L_p^{|m|}$ are the associated Laguerre polynomials. The normalisation constants of the LG modes are given by:

$$C_{mp} = \sqrt{\frac{2p!}{\pi(|m| + p)!}}.$$

Of particular interest for our purposes is the Gouy phase, $\exp[-i(2p + |m| + 1) \tan^{-1}(z/z_R)]$, which describes the phase change as the beam moves through the beam waist, situated at $z = 0$.

On propagation from the beam waist to the far field the term $\tan^{-1}(z/z_R)$ changes from 0 to $\pi/2$. The decomposition of the fractional state in Eq. (1) into integer OAM states uses odd and even values of m . As p has to be an integer it is not possible to have the same Gouy phase for all modes in the superposition, but we can limit the number of different Gouy phases to two, one for even values of m and one for odd values. This can be achieved by choosing appropriate p indices for each LG mode of the superposition. A similar technique has been used earlier to achieve a self-imaging effect [17], where by using superpositions of only odd values of m or only even values of m , the same Gouy phase could be obtained for all the constituent modes. We make use of this idea later in section 6 when we discuss light beams with fractional OAM which are structurally stable on propagation.

The decomposition in Eq. (1) includes an infinite number of integer OAM states, but the optical realisation as a superposition of laboratory beams is restricted by the apertures in the experiment. For a given circular aperture of radius R we require $kR \gtrsim |m|$ for propagating modes [18]. We thus denote the finite number of contributing modes in the superposition by n_{modes} . For every value of M our distribution of the $|c_m[M(\alpha)]|^2$ is peaked around the nearest integer to M (see Figure 1). For $\mu = 1/2$ the modulus square of the coefficients either side of M is equally high. The finite superposition of LG modes is thus centred around the nearest integer to M :

$$\Psi_{M(\alpha)}(\rho, \phi, z) = \sum_{m'=m_{\min}}^{m_{\max}} c_{m'}[M(\alpha)] u_p^{m'}(\rho, \phi, z). \quad (5)$$

The smallest value of m' in the superposition is determined by $m_{\min} = \text{Rnd}[M - n_{\text{modes}}/2]$, whereas the largest value is given by $m_{\max} = m_{\min} + n_{\text{modes}} - 1$. Here Rnd denotes rounding up to the nearest integer greater than M for $\mu \geq 1/2$ and rounding down to the nearest integer smaller than M for $\mu < 1/2$. It is important to note that $0 \leq \mu < 1$, that is μ is not negative. A negative value of M , say $M = -6.5$ has an integer part of $m = -7$ and a fractional part of $\mu = +0.5$. By setting the mode index p for each m' in the superposition Eq. (5) to

$$p_{m'} = \text{Floor} [(|M| + (n_{\text{modes}}/2) - |m'|)/2]. \quad (6)$$

we can ensure that every LG mode has one of two different Gouy phases. Here Floor(q) gives the nearest integer smaller than, or equal to, q . A graph of the values for p and the resulting sum $2p + |m| + 1$ can be found in Figure 1. The distribution of the p indices depends on the total number of modes in the superposition, and therefore it is not possible to add more modes to a given superposition without having to adjust all Gouy phases. This is because for every mode the sum $2p + |m| + 1$ has to be equal to $|m_{\max}| + 1$ or $|m_{\min}|$.

Although a finite set of modes in the superposition Eq. (5) does in general give a non-integer mean value for the OAM, it is not an exact representation of the state from Eq. (1). However, the distribution of the coefficients $|c_m|^2$ in Figure 1 shows that modes with an OAM index m very different from M contribute only little to the superposition. The approximation can in principle be made arbitrarily good by adding more and more modes. However, any experimental realisation will be limited by the difficulties in reproducing the superposition. More modes lead to higher p indices and therefore to a larger intensity pattern with more phase discontinuities associated with the ring structure of the LG beams. Fitting a larger structure on the finite array of programmable pixels of the SLM requires a reduction of the beam waist which in turn leads to a reduction in resolution of the phase and intensity structures on the SLM. In the Appendix A we discuss the effect of a finite number of modes in the superposition on the quantum theoretical properties of the non-integer OAM state.

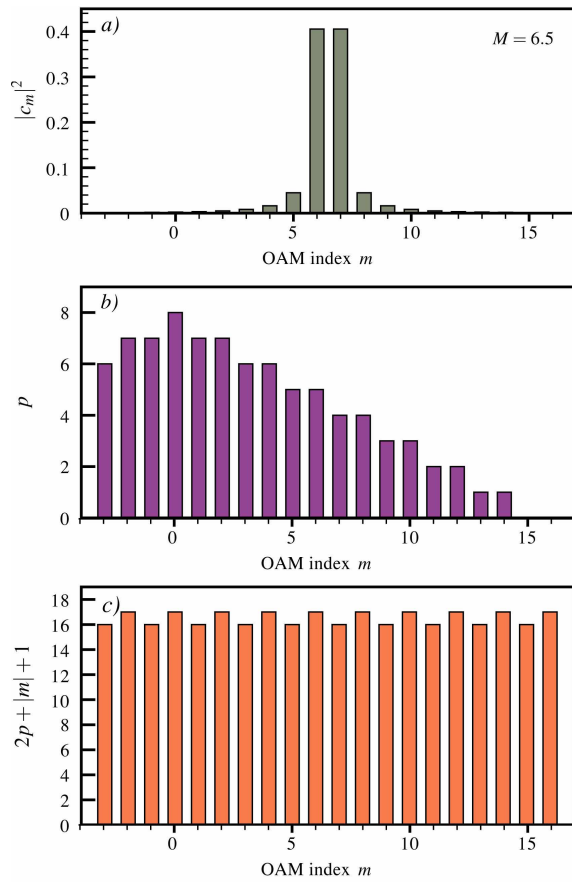


Fig. 1. Fractional OAM beam with $M = 6.5$ realised as the superposition of 20 LG modes. *a)* The distribution of the modulus square of coefficients c_m . *b)* The number of total modes in the superposition, determines the distribution of the indices p for the contributing LG modes. *c)* The annular index p is chosen such that the sum $2p + |m| + 1$ takes on one of two values, giving only two different Gouy phases in the superposition at each propagation distance.

3. Experimental generation of non-integer OAM light beams

Rather than using several optical elements to generate each LG modes separately we employ a single SLM programmed with a hologram that sets the phase and intensity structure for the superposition. A blazed grating is also included in the hologram to separate angularly the first diffraction order. The formula for the resulting phase distribution of the hologram in rectilinear coordinates $\Phi(x,y)_{\text{holo}}$ is given by [4]

$$\Phi(x,y)_{\text{holo}} = [(\Phi(x,y)_{\text{beam}} + \Phi(x,\Lambda)_{\text{grating}}) \bmod 2\pi - \pi] \text{sinc}^2[(1 - I(x,y)_{\text{beam}})\pi] + \pi. \quad (7)$$

Here, $\Phi(x,y)_{\text{beam}}$ is the phase profile of the superposition at the beam waist for $z = 0$ and $\Phi(x,\Lambda)_{\text{grating}}$ is the phase profile of the blazed grating which depends on the period of the grating Λ . The two phase distributions are added modulo 2π and, after subtraction of π , multiplied by an intensity mask. In regions of low intensity the intensity mask reduces the effect of the blazed grating, which in turn leads to reduced intensity in the first diffraction order. The mapping between the phase depth and the desired intensity is not linear but rather given by the trigonometric sinc function. In Figure 2 we illustrate the algorithm of the hologram designed to generate a superposition according to Eq. (5) for 10 modes and $M = 6.5$.

Figure 3 depicts the experimental arrangement. The hologram is implemented using a computer controllable spatial light modulator (SLM). The light beam is produced with a HeNe laser, which has been expanded with help of the lenses f_1 and f_2 to illuminate the SLM evenly (see Figure 3). The recording of the phase profiles requires a reference beam which is coupled out from the illumination over a beam splitter and which is then reflected on mirror M_1 . This reference beam can be blocked by an electronic shutter. Depending on whether the shutter is closed or open, either the reflected light from the SLM or its interference with the reference beam is imaged by lens f_3 onto a spatial filter which only transmits the first positive diffraction order. The light is then passed through a collimation lens f_4 onto the mirrors M_3 and M_4 , which are mounted on a movable track to select a propagation distance, which is then imaged by lens f_5 onto a CCD array to record the image. The process of opening and closing the shutter, moving the mirror mount to the correct position for the desired propagation distance and recording the image is automated by use of a computer running a Labview programme. The programme also generates the desired hologram. In the setup used to record the experimental results we were able to take cross sections of the intensity and phase of the beam over a propagation distance from about $z = 0$ to $z = 4z_R$. By adjusting the beam waist, longer propagation distances are feasible, but at four Rayleigh ranges, the phase change induced by the Gouy phase is already close to its maximum value.

4. Phase and intensity profiles

The intensity and phase profiles of light emerging from a half-integer phase plate change drastically on propagation [11, 12]. In contrast, our synthesised light beams show small changes in the phase and intensity profiles on propagation from the near field to the far field. To compare the phase and intensity profiles without dilation due to the increase in the Gaussian spot size we introduce scaled coordinates $x/w(z)$ and $y/w(z)$. In Figure 4 we compare numerical and experimental pictures of the propagation of the beam. The series of graphs shows the intensity and phase profiles at the waist plane and after propagation of 2 and 4 Rayleigh ranges ($z = 2z_R$ and $z = 4z_R$) for $M = 6.5$ and a superposition of 10 LG modes according to Eq. (5). One can see that the intensity profile shows a rotation by $\pi/2$, which we attribute to the difference in the Gouy phase between the waist plane and the far field. This difference, however, affects only the modes in the superposition for which the sum $2p + |m| + 1 = 17$. The other modes satisfy the self-imaging condition as the phase difference between the waist plane and the far field is an

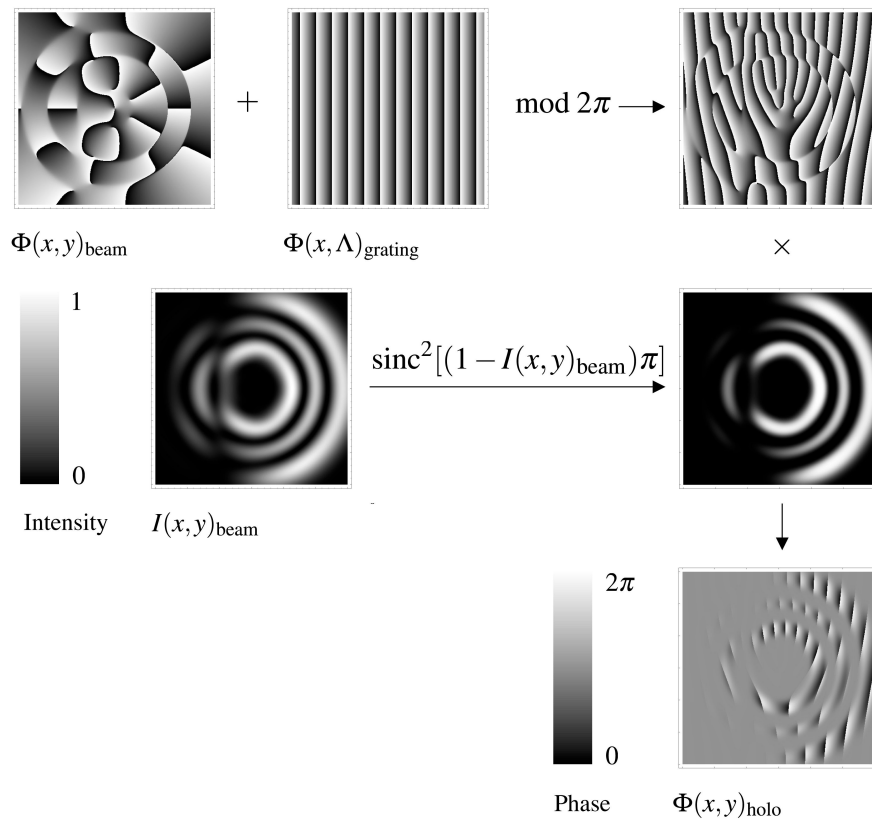


Fig. 2. Illustration of the steps necessary, implicit in Eq. (7), to generate the hologram which produces the non-integer OAM beams according to Eq. (5). A carrier phase representing a blazed grating is added to the phase of the superposition modulo 2π . This combined phase is multiplied by an intensity mask which takes account of the correct mapping between phase depth and diffraction intensity. The result is a hologram containing the required phase and intensity profiles. The various cross-sections are plotted over a range $\pm 3w_0$.

integer multiple of 2π . The self-imaging condition is specific for this particular superposition, while a rotation of the intensity structure on propagation is characteristic for our generic superposition if a sufficiently large number of modes is included. A rotation of the intensity structure can not always be associated with the Gouy phase [19]. It is interesting to note that the ‘cap’ of the open ring structure in the intensity profile for $z = 0$ corresponds to the orientation of the fractional phase step α (in all examples we have set $\theta_0 = -\pi$ and $\alpha = 0$). Taking more modes in the superposition into account leads generally to more rings. This is because a higher total number of modes leads to a higher p index for those modes which contribute most to the superposition according to Eq. (6).

The phase profiles depend, to a greater extent, on the number of modes included in the superposition. The initial vortex structure at the beam waist is dominated by the two modes which contribute most to the superposition (for our example of $M = 6.5$ the LG modes with $m = 6$ and $m = 7$). As long as there are more than two modes in the superposition, one vortex of charge ± 1 will form along the orientation of α . Depending on the number of modes in the superposition the high charge vortices on axis split up into simple 2π vortices distributed around

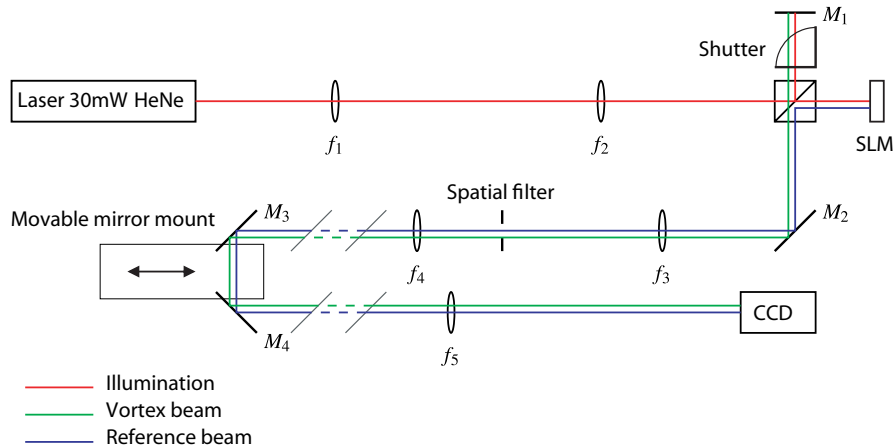


Fig. 3. Schematic representation of the experimental setup. To record the intensity and phase profiles an electronic shutter either blocks the reference beam or lets it through. The mirrors M_3 and M_4 are mounted on a rack which can be moved to select the desired propagation distance. The SLM, the shutter, the movement of the track and CCD array are all automated.

the optical axis. The picture is a bit different if the superposition contains the mode with $m = 0$ as this mode adds on-axis intensity and leads always to a split of the high charge vortices. This effect is more pronounced if M is small because then the mode with $m = 0$ contributes more to the superposition. Figure 5 shows the intensity and phase profiles for a superposition of 6, 10 and 20 modes for $M = 6.5$. On propagation the vortex structure changes and aligns itself roughly along a line which is rotated by $\pi/2$ from the orientation of α . This will become clearer in the figures in the next section, where we compare theoretical and experimental pictures of the vortex structure on propagation.

5. Vortex structure

Phase profiles at different propagation distances give only a limited picture of the spatial form of the vortices. In Figure 6 we show a three dimensional plot of the nodal lines traced by the vortices. The graph compares the numerical calculation with the experimental results. Both plots are produced by searching the phase profiles for vortex positions at different propagation distances. The vortices are traced from the waist plane at $z = 0$ to a propagation distance of $z = 2.5z_R$. One can see that the experimental result is in very good agreement with the numerical simulation and that the topological aspects of the vortex structure are correctly reproduced. The graphs show quite clearly the line of vortices which forms on propagation roughly 90 degrees rotated from the orientation of the cap. Another feature is the presence of 'hairpin' curves, a pair of vortices which are joined at a turning point. Shorter hairpins appear in the dark rings and extend only for a small fraction of a Rayleigh range, but one hairpin connects the vortex in the direction of α with a vortex from the ring structure and extends to a propagation distance of over one Rayleigh range. This vortex pair is important for the formation of a new vortex on changing M through the half-integer value. Interestingly, a new hairpin is also formed at the same position, $z \approx 2z_R$.

The good agreement between the numerical and experimental results in the vortex structure is an indication that the desired and generated beam conform to a high degree as the vortex structure is very susceptible to perturbations [11]. The numerical calculations predict for example

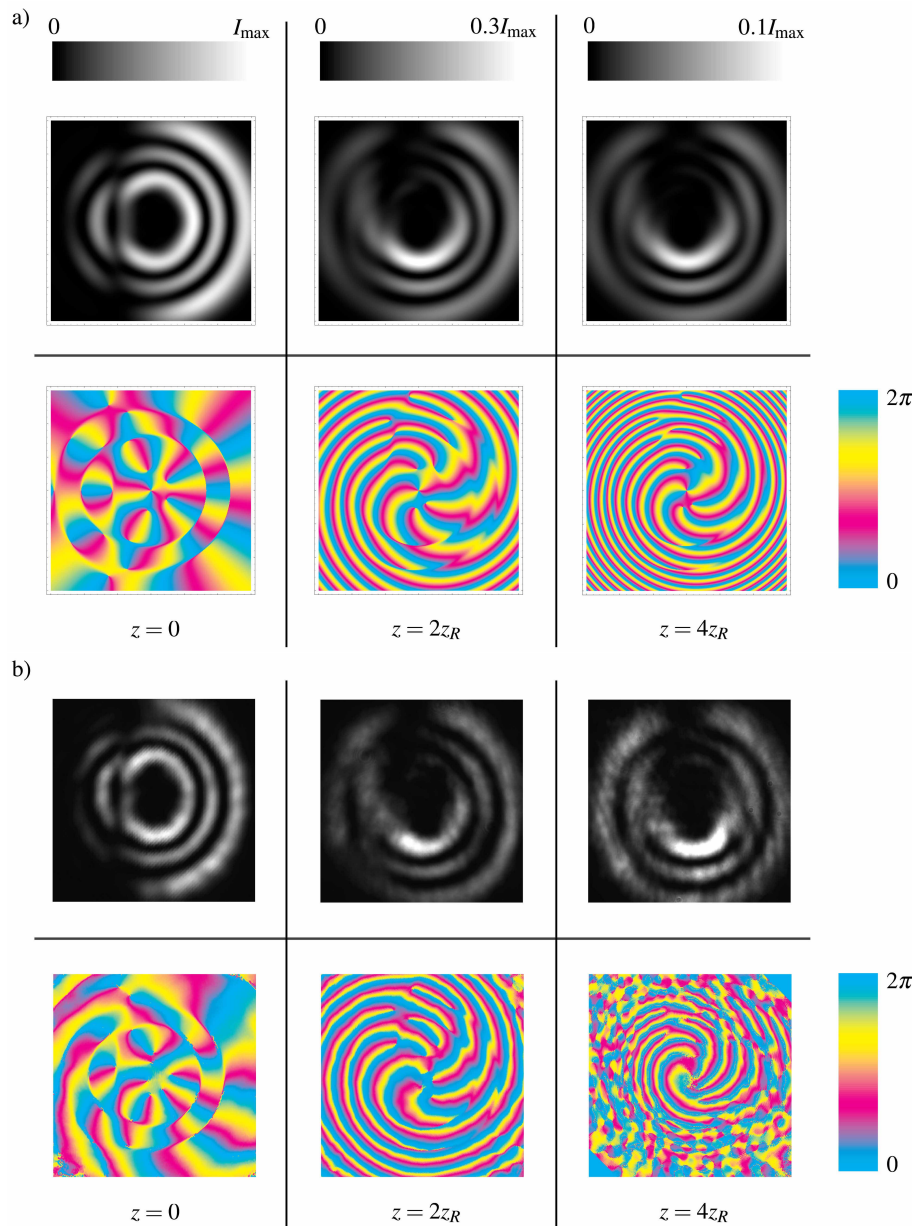


Fig. 4. Intensity and phase profiles on propagation for a superposition of 10 modes and $M = 6.5$. *a)* The sequence of numerical plots for three different propagation distances at $z = 0, 2z_R$ and $z = 4z_R$ shows the changes in the phase and intensity on propagation from the waist plane into the far field. The various cross-sections are plotted over a range $\pm 3w(z)$ for each value of z . *b)* shows the corresponding experimental profiles.

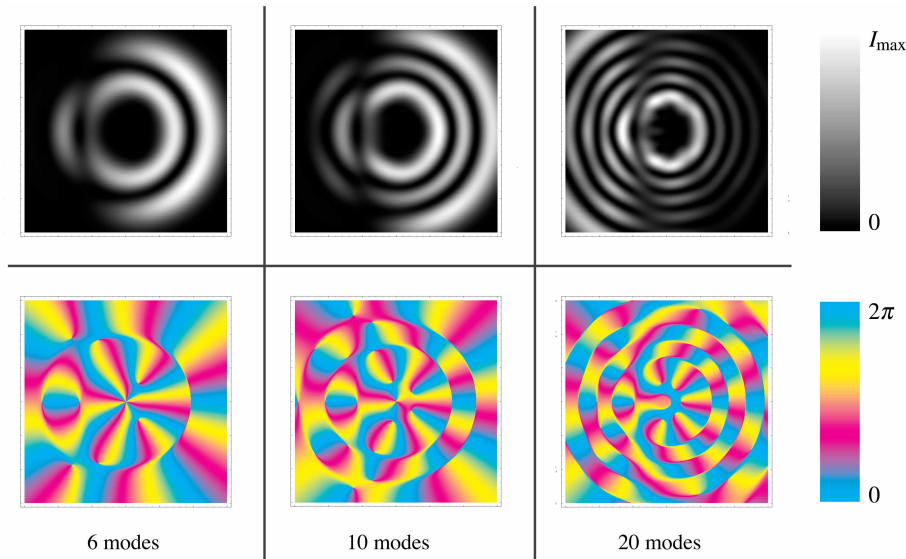


Fig. 5. Theoretical intensity and phase profiles at the beam waist for different numbers of modes in the superposition. The various cross-sections are plotted over a range $\pm 3w_0$. Adding more modes leads to a higher p index for the dominant LG modes. This explains why the intensity profiles show a larger number of rings for more modes in the superposition. Between each ring of an LG modes is a π phase step which explains the higher number of rings in the phase profile. Increasing the number of modes also leads to a separation of the on-axis high charge vortex in several vortices with charge ± 1 .

the existence of either a vortex of charge 2 or two vortices with charge 1 in the centre. The experimental results show that these two vortices start to spiral around each other on propagation, which indicates a small perturbation of the charge 1 vortices.

6. Structurally stable light beams with fractional OAM

Using a superposition of two fractional OAM states with a π difference in the orientation α , it is possible to create a beam which, when decomposed into OAM states, has either only odd or only even m . By adjusting the p values of the superposition modes, a uniform Gouy phase can be obtained. The corresponding light beam, apart from dilation, propagates unchanged and is hence structurally stable. We construct such a beam by setting

$$|M_+(\alpha)\rangle = \frac{1}{\sqrt{2(1 + \cos(\mu\pi))}} (|M(\alpha)\rangle + |M(\alpha + \pi)\rangle). \quad (8)$$

For an even integer part of M the state $|M_+(\alpha)\rangle$ gives a superposition of even modes, while for an odd integer part of M the decomposition contains only odd modes. The normalisation of these states depend on μ as only for $\mu = 1/2$ fractional states are orthogonal if the difference in orientation is π . Because of the interference between the two constituent beams, the total OAM mean value is different from the single states $|M(\alpha)\rangle$ [10], and is given by

$$\bar{M} = \frac{2M\pi[1 + \cos(\mu\pi)] - \sin(2\pi\mu) - 2\sin(\mu\pi)}{2\pi[1 + \cos(\pi\mu)]}. \quad (9)$$

We can prepare a stable approximation to the superposition (8) by limiting the number of contributing modes, as described in section 2, and choosing the values of p to produce a unique

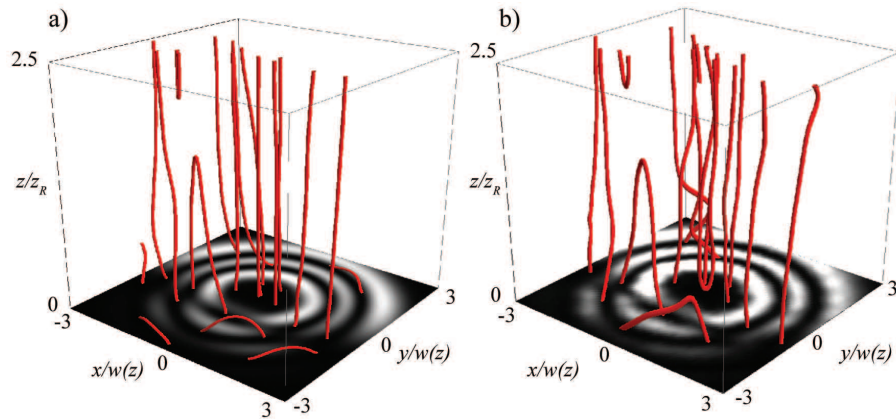


Fig. 6. Three dimensional view of the vortex structure for a superposition of 10 modes and $M = 6.5$. *a)* shows the numerical results and *b)* the experimental measurements. Both vortex structures exhibit a number of topological features such as formation of a line of vortices and the existence of ‘hairpins’, connected nodal lines which cumulate in a turning point.

Gouy phase. The resulting beam should be stable on propagation. For our example of $M = 6.5$ and 10 modes in the representation of $|M(\alpha)\rangle$ and $|M(\alpha + \pi)\rangle$ only the 5 even modes for $m = 2, 4, 6, 8, 10$ are left. Including 10 even modes in the representation of $|M(\alpha)\rangle$ would lead to a much higher number of rings. As with Figure 4 we adopt a radial coordinate such that divergence of the beam is suppressed. One can see clearly in Figure 7 that the scaled profiles remains unchanged on propagation. The phase profile shows roughly an m -fold rotational symmetry. This is because the superposition is now dominated by the mode with m equal to the integer part of M . The positions of the phase singularities remain unchanged as predicted.

7. Conclusion

It is well-established that beams with vortices can carry OAM and in particular that the LG modes carry an OAM of $m\hbar$ per photon, where m is the charge of the on-axis vortex [5]. Vortices of fractional strength can be incorporated only by also introducing a discontinuity in the beam. This follows directly and simply from the requirement that the field amplitude must be everywhere single valued. It is the discontinuity that leads to the break-up of the central vortex structure and to the consequent change in the beam profile on propagation [9, 10].

We have shown that stable fractional OAM beams can be generated by using the radial degree of freedom. The changes upon propagation exhibited by conventional fractional OAM beams can be attributed to interference between the contributing LG modes with different Gouy phases. These differences can be suppressed, however, by selecting LG modes with appropriate radial indices, p , for each contributing value of m [17]. Our work has demonstrated the existence of simple superpositions of LG modes resulting in fractional OAM, but which undergo only a $\pi/2$ rotation on propagation from the beam waist to the far field, or even maintain their structural stability completely.

The structural stability of our beams is attractive for the generation or measurement of fractional OAM states in both the classical and quantum regimes. One potential application is in the measurement and manipulation of fractional OAM for entangled photon pairs [13].

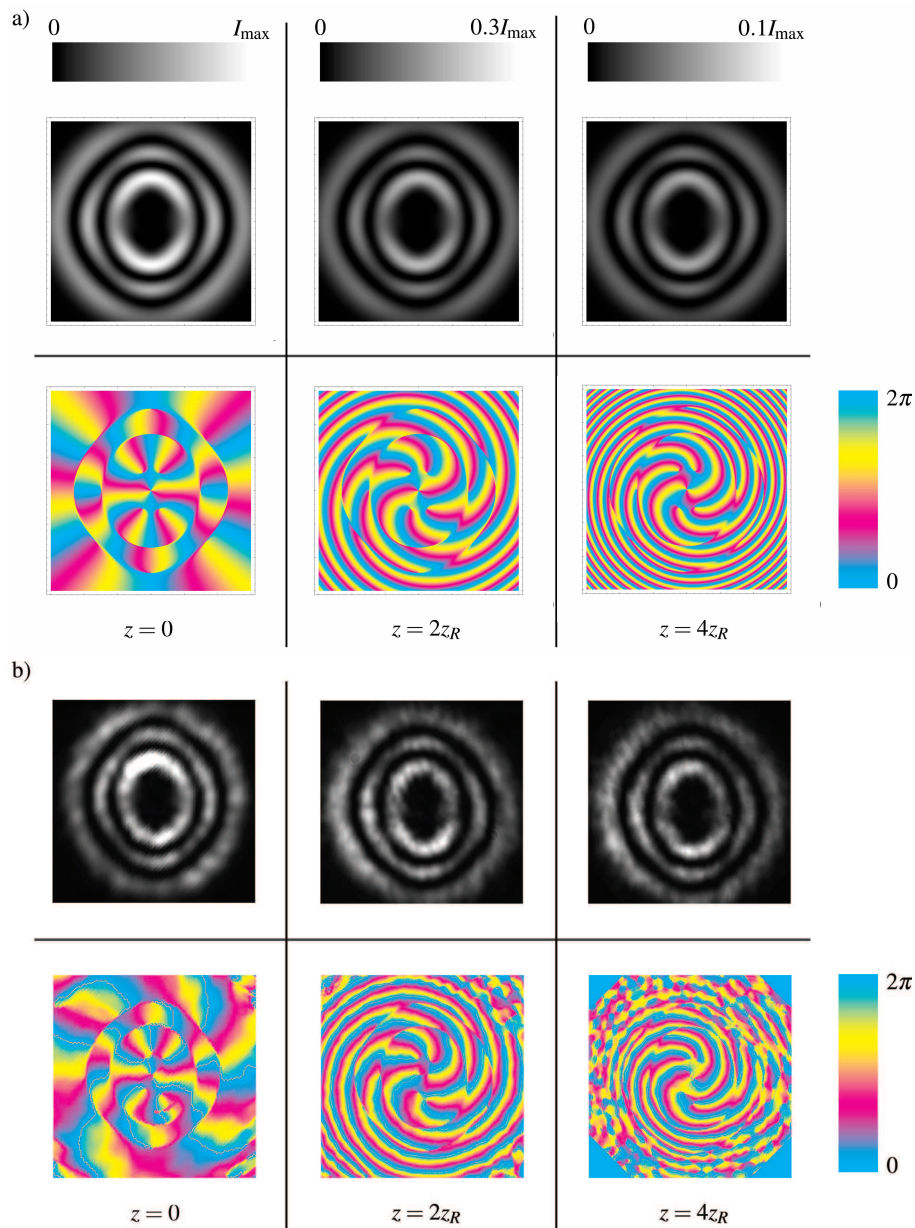


Fig. 7. Intensity and phase profiles for a superposition of light beams in which all modes have the same Gouy phase. The superposition consists of 5 modes and $M = 6.5$. *a)* shows the numerical results for three different propagation distances of $z = 0, 2z_R$ and $4z_R$. The various cross-sections are plotted over a range $\pm 3w(z)$. Apart from dilation the intensity structure remains invariant. In the phase profiles one can see that in the scaled variables the vortices remain at the same locations. *b)* shows the experimental results.

Acknowledgements

This work was supported by the Leverhulme Trust, the Royal Society and the Wolfson Foundation.

A. Non-integer OAM states

Non-integer OAM states depend on the orientation of the phase step α . For odd half-integer values of M the overlap between states with a π difference in the orientation α vanishes [13]. Using only a finite number of states gives only an approximation and changes the properties of the non-integer OAM states. Including more states in the superposition improves the approximation and the properties of the original OAM states are recovered. It is interesting to quantify the effect a finite superposition has on the properties of the non-integer OAM states.

As a test, we calculate the overlap $\langle M(\alpha)|M(\alpha')\rangle$ for states defined as a finite superposition of OAM eigenstates in analogy to Eq. (5):

$$|M(\alpha)\rangle = \sum_{m'=m_{\min}}^{m_{\max}} c_{m'}[M(\alpha)]|m'\rangle. \quad (10)$$

The overlap of two such states for equal M is given by

$$\langle M(\alpha)|M(\alpha')\rangle = \frac{\exp(i\mu\beta)}{2\pi} (1 - \cos(2\pi\mu)) \sum_{m'=m_{\min}}^{m_{\max}} \frac{\exp[i(M-m')\beta]}{(M-m')^2}, \quad (11)$$

where we have set $\beta = \alpha - \alpha'$. We evaluate the modulus square of the overlap for different total numbers of OAM states in the superposition over a 2π range for β . For non-integer OAM states, defined on an infinite space this quantity is independent of the m , the integer part of M . The same is true for the finite set which can be seen if we introduce a new index $n = m - m'$, where m is the integer part of M . The sum in Eq. (11) is transformed to

$$\langle M(\alpha)|M(\alpha')\rangle = \frac{\exp(i\mu\beta)}{2\pi} (1 - \cos(2\pi\mu)) \sum_{n=n_{\min}}^{n_{\max}} \frac{\exp[i(n+\mu)\beta]}{(n+\mu)^2}, \quad (12)$$

where the summation ranges from $n_{\min} = \text{Rnd}(\mu - n_{\text{modes}}/2)$ to $n_{\max} = n_{\min} + n_{\text{modes}} - 1$. This sum no longer contains m , which establishes that the overlap is independent of the integer part of M .

The graph in Figure 8 shows $|\langle M(\alpha)|M(\alpha')\rangle|^2$ for $\beta = \alpha$ (with α between 0 and 2π). As in the main part of the paper we restrict our analysis to odd half-integer values of M . Although the form of the overlap does change with the number of states in the superposition, it is clear that for $\beta = \pi$, the states are orthogonal to a very good degree even if calculated on a very limited set of states. The inset shows that the approximation improves only for more than ten states in the superposition.

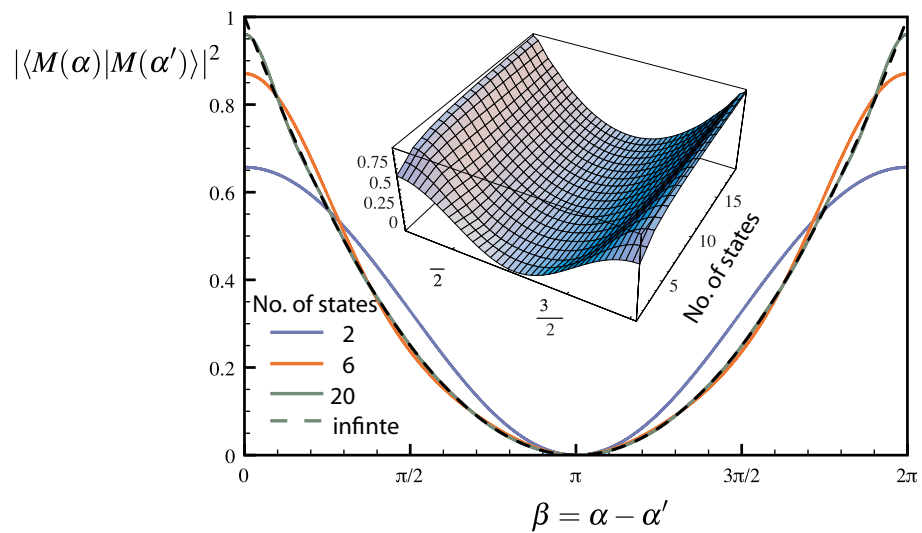


Fig. 8. Graphs showing the modulus square of the overlap $\langle M(\alpha)|M(\alpha')\rangle$ for different values of $\beta = \alpha - \alpha'$. The overlap is calculated on a finite set of OAM eigenstates and for different values of the total number of OAM eigenstates to show the effect a finite number of states has on the properties of the non-integer OAM states.